RPF
Excerpt from LA-12934-MS.

(14) 54404

MEASUREMENT AND ANALYSIS OF ROCK FRACTURES IN THE TSHIREGE MEMBER OF THE BANDELIER TUFF ALONG LOS ALAMOS CANYON ADJACENT TO TECHNICAL AREA-21

by

K. H. Wohletz

A total of 1662 fractures was measured in unit 2 of the Tshirege Member of the Bandelier Tuff along a section of Los Alamos Canyon adjacent to TA-21. Beginning 1200 ft east of Omega Site (TA-2), the section extends eastward 7312 ft to near the end of DP mesa. Photomosaic maps were constructed to document each fracture, and measurements were entered into an RS/1 database for analysis. Background linear fracture density averages around 20 fractures/100-ft interval with a notable increase to about 70 fractures/100 ft over a zone that extends ~1500 ft east-west and is centered directly south of MDA V. Within this same zone, mean fracture apertures increase from background values of ~0.8 to ~1.25 cm. Fractures make up a conjugate set of NW and NE strikes. Overall, the average strike is about N12E, but the 988 NE-trending fractures show a mean strike of N43E, and the 674 NW-trending fractures have a mean strike of N33W. Fracture dips are generally steep, averaging between 73°N and 70°S. Both fracture mean strikes and dips show rotations of several degrees in the most highly fractured zone.

INTRODUCTION

Abundant rock fractures extend throughout the Tshirege Member of the Bandelier Tuff underlying DP Mesa (Fig. 1) at TA-21. These fractures are important geological features because they constitute potential pathways for contaminant infiltration from MDAs on the mesa; they also affect slope stability along the canyon margins. This report documents an extensive field survey of exposed fractures carried out at TA-21 in 1992. It builds upon previous fracture studies conducted by Vaniman and Wohletz (1990) and employs the detailed procedure developed in that study.

The origin of the fractures in the Bandelier Tuff has never been described fully. Work by Vaniman and Wohletz (1990) suggests, by analogy to numerous other studies of welded tuffs and by consideration of tectonics of the Pajarito Plateau (Gardner and House, 1987), that most of the fractures can be explained by brittle failure of the tuff during cooling contraction. Tectonic movement over the last million years along the Pajarito fault system caused subsequent fracture extension and development in the tuff. Because the exact origin of the fractures is still in question, this study does not attempt to classify fractures according to their geological origins.

Received by ER-RPF
JUN 03 1996
Dic

10449

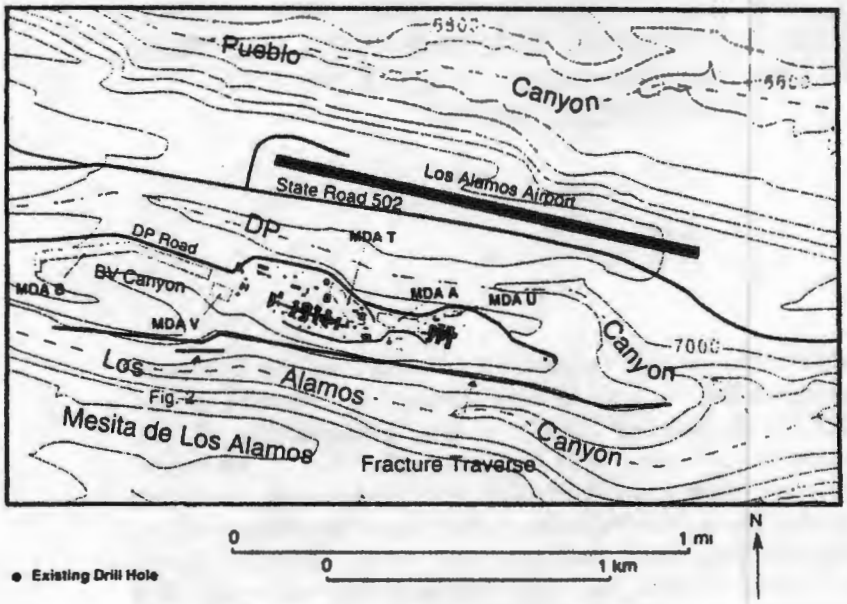

Fig. 1. Topographic map of TA-21. The fracture traverse extends along the north wall of Los Alamos Canyon from 1200 ft east of Omega Site (not shown) to 8512 ft east of Omega Site. Fourteen photomosaic fracture maps cover this traverse. Figure 2 shows an example of the photomosaic maps for the area adjacent to MDA V.

METHODS

The methodology consists of three phases, as outlined by the *SOP for Fracture Characterization* (LANL-ER-SOP-03.06): (1) photographic documentation of area or traverse along which fractures will be characterized and construction of a photomosaic map base, (2) measurement and plotting of fracture dimensions on the photomosaic map, and (3) statistical analysis of fracture data by the procedures described below.

The south-facing cliff exposures along Los Alamos Canyon were chosen for this study because they provide the only continuous vertical exposure of the Tshirege Member of the Bandelier Tuff beneath TA-21 (Fig. 2). Unit 2 of Vaniman and Wohletz (1990) is partly welded along this traverse and shows the best exposure of fracture surfaces; consequently, the results of this study are from unit 2. The documented section begins 1200 ft east of the Omega Site (TA-2) access gate to the canyon and continues 7312 ft to the east.

Photo Documentation

When unit 2 of the Tshirege Member was photographed, successive stations at the base of the unit (where slopes are accessible) were set up so that focal distances of 40 to 60 ft were maintained and photographs had ~ 20% overlap. Because of the curvature of the cliff face and its irregular vertical extent, each photograph covered between 30 to 50 ft of lateral exposure; scales added to the photomosaics reflect this variable lateral scale. After construction of the photomosaic, tracing paper was overlaid to make a map of outcrop features, including key topographic points such as cliff tops and bottoms, prominent fractures, and geographic objects such as buildings, trees, and large signposts. This map was attached to the base of the photomosaic so that there is a 1:1 correspondence between mapped and photographed features. The 7312-ft traverse required 14 individual photomosaic maps, each covering ~500 ft of lateral exposure.

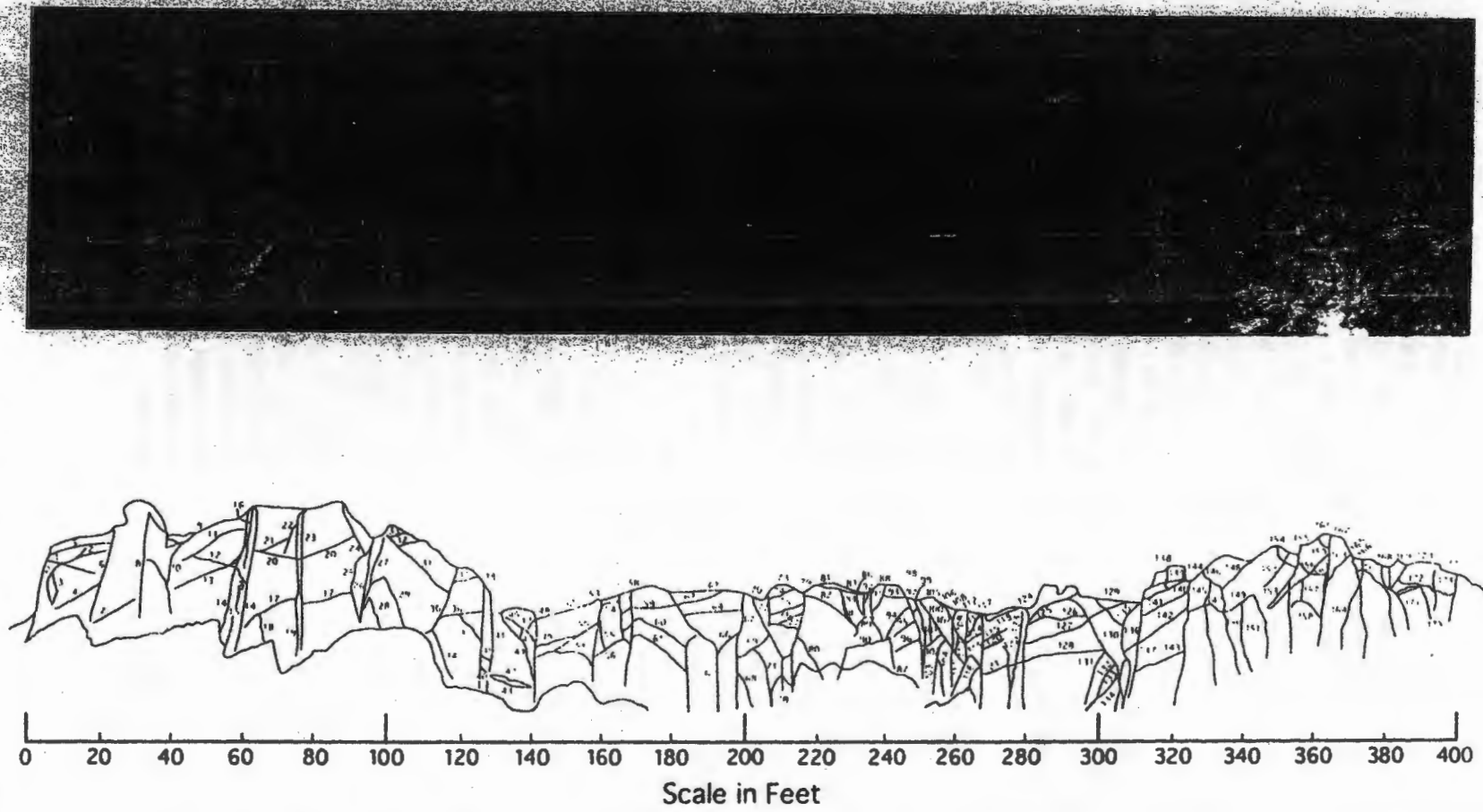

Fig. 2. Photomosaic and fracture map of the north wall of Los Alamos Canyon in the vicinity of MDA V. (See Fig. 1 for location of photograph.)

Fracture Measurement

The horizontal scale for the fracture maps was determined by measuring distance on the topographic map between topographic points identified on the photomosaics. This scale was then placed on each map to show the distance between mapped features. Because of the exposure irregularities in cliff face described above, this scale will have an error of ±10% of each map's total width.

Starting from one end of the fracture traverse, each fracture was sketched on the map and designated by a number. These numbers increase from west to east and are pertinent only to the photomosaic map on which they are shown (for example, fracture numbers 1 though 80 of photomosaic map 1, fracture numbers 1 through 66 of photomosaic map 2, etc.). The location of each fracture is its average point of intersection on the map. All observed fractures have been recorded with some parallel sets too closely spaced to be given individual numbers on the map, but nonetheless they are recorded in the database. Fracture strike and dip were measured to an accuracy of ±2° with the Brunton compass, and fracture opening width was measured perpendicular to fracture surfaces. In cases where fractures could not be safely accessed, standard application of Brunton compass techniques were applied; these require measurements using the compass alignment sights with cautious observation of the relationship between true and apparent orientations.

Fracture Data Base and Analysis

The fracture data recorded in the field notebook were entered into a database, which allowed application of several statistical procedures. The database consists of a table with a column for each fracture, listing the fracture's number designation, horizontal location on the fracture map, dip and strike, and aperture. From these data, several other columns are statistically calculated: (1) a linear fracture density calculated as a moving average by counting the number of fractures contained in a given distance interval (10 and 100 ft) that is centered on each fracture, (2) a cumulative fracture width over a specified interval (10 and 100 ft) that is centered on each fracture, and (3) the relative dip of fracture from vertical, (negative values indicate southerly inclinations). Because fractures in the Bandelier Tuff show apparent NW- and NE-strike groupings and cross-cutting relationships suggest that these two groups are coeval, I have considered fractures to represent a conjugate set. Accordingly, additional columns for the table are separately calculated for each of the three above columns for each conjugate set. This conjugate relationship is an hypothesis I attempt to support in later data analysis. Numerical procedures for the above include: (1) calculation of linear fracture densities for several different distance intervals, taking into account section end effects by extrapolating the gradient of density with distance, (2) transformation of dip measurements to degrees from vertical, and (3) computation of cumulative fracture widths for 10- and 100-ft distance intervals. Although more sophisticated statistical analyses can be applied to these data, those used are sufficient to characterize the fractures.

Fracture data were then displayed on several different plots:

(1) fracture density (10- and 100-ft intervals) *vs* horizontal distance along the traverse;
(2) histograms of fracture strike;
(3) fracture strike *vs* horizontal distance, where positive strikes represent strike in degrees east of north and negative strikes are west of north (these data are smoothed using the RS/1 data-smoothing option to show the trend of northeast and northwest fracture sets as well as the overall trend of all fracture strikes);

(4) fracture dips *vs* horizontal distance, where vertical plots at zero, dips toward the northeast or northwest are positive inflections from vertical, and southerly dips are negative inflections from vertical (again, smoothing of data shows average trends for fracture sets);
(5) fracture widths *vs* horizontal distance with smoothed trends for fracture sets;
(6) cumulative fracture widths (per 10-ft intervals *vs* horizontal distance with smoothed trends for fracture sets; and
(7) fracture widths >10 cm *vs* horizontal distance.

RESULTS AND ANALYSIS

A total of 1662 fractures was documented and measured along the 7312-ft section located along Los Alamos Canyon, as is shown in Fig. 1. An example photomosaic and fracture map documenting part of this section is shown in Fig. 2. The measurements for each of the numbered fractures on this map are archived in a computer database, as described above. The tabulated data for fracture strike, dip, and aperture are shown statistically in Tables 1, 2, and 3.

Fracture Density

In general, the background spacing of fractures is ~5 ft, which is similar to a value found for nearby areas in the Bandelier Tuff, by Vaniman and Wohletz (1990). However, over the zone from 2500 to 4000 ft east of Omega Site, the fracture spacing is much closer (1 to 2 ft). Figure 3 is a plot of linear fracture density for 10- and 100-ft intervals centered around each fracture. Note that very little lateral variation in fracture density is immediately apparent for the data plotted for 10-ft intervals; this represents the density generally apparent to an individual viewing the section while in the field. The 100-ft interval is arbitrarily chosen

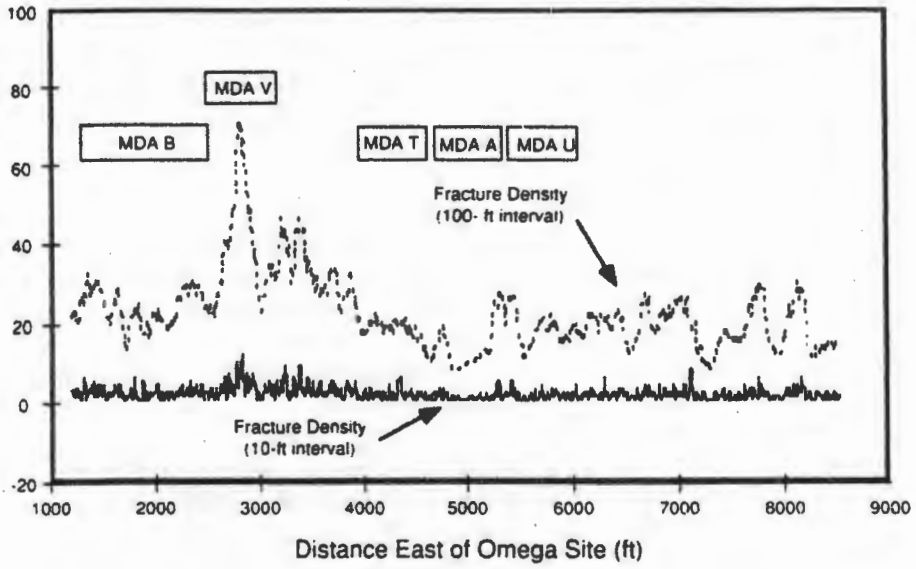

Fig. 3. Plot of linear fracture density vs distance east of Omega Site. The curves show fracture density over 100- and 10-ft intervals.

to represent the width of potential tectonic features. Data plotted for 100-ft intervals shows a background density of ~20 fractures per 100 ft; a notable increase at horizontal locations between 2500 and 4000 ft that reaches a high of about 75 fractures/100-ft interval.

The notable rise in fracture density occurs abruptly 2500 ft east of Omega site and then falls off more gradually to the east, reaching background values at ~4000 ft. This zone corresponds to a fracture zone running N-S that Vaniman and Wohletz (1990) mapped but did not document by fracture studies. It likely represents a fabric of the Pajarito fault system. The zone's northerly projection runs directly through MDA V at TA-21. In all, 554 fractures were documented in this 1500-ft-wide fracture zone, whereas 310 fractures were found over a distance of 1300 ft to the west, and 828 fractures were found over a distance of 4512 ft east of the zone.

Fracture Strikes

Because observed fractures are likely to have been formed during the cooling contraction of the Bandelier Tuff, a conjugate system with 60° fracture intersections should be expected. This simple hypothesis is complicated by the fact that the tuff compacted over a preexisting topography with a strong E-W fabric, which would cause a dominant N-S strain component to be accommodated by the fractures. Figure 4a is a rose diagram of fracture strike frequency measured along the approximately E-W trend of Los Alamos Canyon. Because of its orientation, this canyon exposes fractures as a sine function of the angle between the fracture strike and the canyon wall; hence, the abundance of E-W trending fractures is greatly reduced. This figure portrays a weak bimodality of fracture strikes with modes in the NW and NE quadrants. The distribution of strikes is generally symmetric around the N-S axis and, because of their mutually cross-cutting relationships, these two modes define a conjugate fracture set.

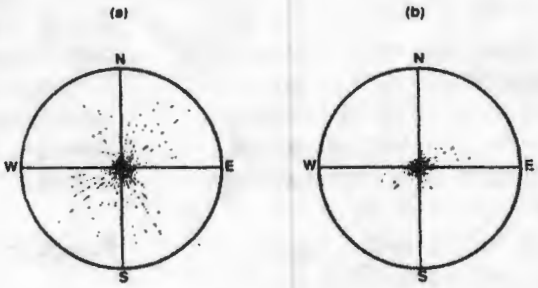

Fig. 4. Rose diagrams of fracture strikes measured in Los Alamos Canyon plotted in 10° classes. (a) Observed distribution of the 1662 fractures measured for which maximum petal magnitude is 140 occurrences. (b) Calculated distribution corrected for angle between fracture strike and the E-W line of Los Alamos Canyon exposures (maximum petal magnitude is 495 occurrences). Here, an additional 1109 fractures were inferred by the relationship of $n = n/\sin \alpha$, where n is the number observed for each class and α is the angle between each class's strike and E-W.

By applying a trigonometric correction for the exposure bias, Fig. 4b shows that there is likely a dominant E-W trend in fracture strikes and that the NW and NE modes are subordinate. If one assumes the dominant E-W fractures shown in Fig. 4b are real, then dominant fracture intersections reproduce 60° angles (~N30W, ~N30E, ~E-W), as expected for a cooling contraction origin.

Because the E-W component is inferred, fracture data are further represented with respect to only the NW and NE strike modes. Table 1 lists fracture strike data for the section, showing that of the 1662 fractures measured, 988 trend NE and 674 trend NW. In Table 1, fractures are differentiated into three zones: those occurring west of 2500 ft (western background), those between 2500 and 4000 ft (fracture zone), and those east of 4000 ft (eastern background). Whereas the NW set shows a mean strike of N33W, the NW set shows a mean of N43E—indicating an average intersection angle with the NE set ~15° greater than the expected angle of 60°. This result is likely a reflection of the dominating influence of E-W

TABLE 1.
FRACTURE STRIKE DATA FOR TA-21[a]

Fracture Set	Number	Mean Strike	Standard Deviation
All Fractures			
NE	988	42.7	±24.5
NW	674	-32.8	±23.1
Background (West)			
NE	182	44.3	±26.8
NW	128	-33.8	±22.0
Fracture Zone			
NE	312	45.0	±24.5
NW	212	-40.6	±25.5
Background (East)			
NE	494	40.7	±23.5
NW	334	-27.4	±20.3

[a] Strikes shown in degrees from due north. NW strikes designated by negative values. Fracture zone corresponds to horizontal distances from 2500 to 4000 ft east of Omega Site.

fractures in calculation of the NE set mean strike. Note the slight rotation of mean strikes west to east over the fracture zone from N44E and N34W to N41E and N27W, respectively. This rotation may represent the influence of tectonic movement on fracture orientations in the fracture zone.

Fig. 5 shows a plot of fracture strikes as a function of horizontal location. In this plot, smoothed curves for the data show average orientations of all fractures, only NE-trending fractures, and only NW-trending fractures. Note in Fig. 5 that azimuths west of due north plot as negative values in degrees. A composite average of all fractures varies between due north and N20E, with the NE set averaging around N40E and the NW set averaging around N30W. There is notable fluctuation of these curves over a zone extending from 2500 to 4000 ft west of Omega Site, which corresponds to the fracture zone with increased fracture density. Over the fracture zone, strikes are divergent (spreading apart), but to the east of this zone, the angle between them stays fairly constant (sympathetic).

Fracture Dips

Fracture dips range from nearly horizontal to vertical; northerly dipping fractures show a mean dip from horizontal of about 74 ± 22° and southerly dipping ones have a mean at about 68 ± 20°. Table 2 lists results of fracture dip data, showing statistics for all fractures both those in the fracture zone (2500 to 4000 ft) and those on either side of the fracture zone (considered background values). Note that dips are shown in degrees from vertical (Table 2, Figs. 6 and 7) so that northerly dips could be averaged with southerly dips (noted as negative values). As with strikes, a NE- and a NW-trending set are designated. Where northerly and southerly dips are not discriminated in Table 2, the greater abundance of northerly dipping fractures gives mean values of 8.5° (N) for both the NE and NW sets. In Fig. 6, fracture dips are plotted against horizontal location. Curves for all fractures, the NE set alone, and the NW set alone are shown with dips indicated as degrees from vertical such that southerly dips plot below 0° (vertical). For most of the section, the NE and NW sets show sympathetic

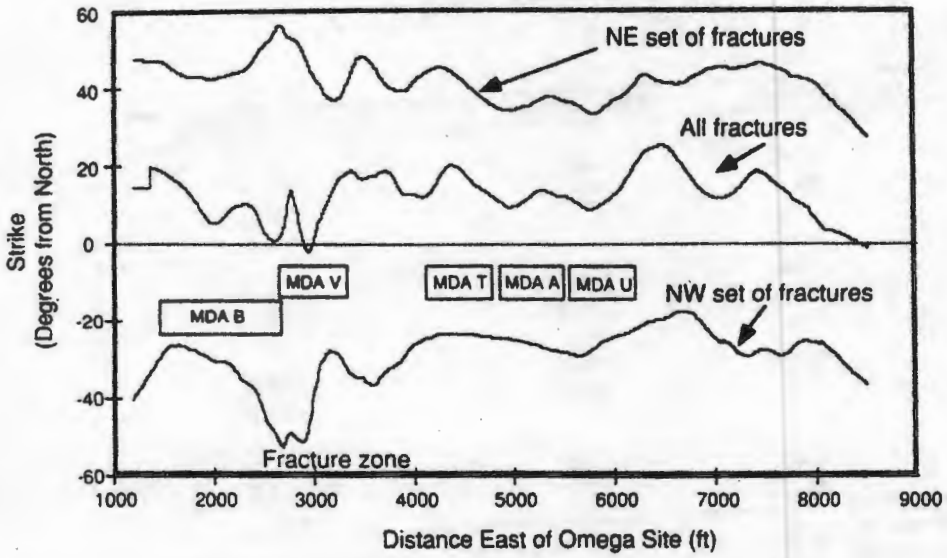

Fig. 5. Plot of linear fracture strikes vs distance east of Omega Site. Curves show smoothed running averages (0.1 smoothed = 162 fractures averaged about each fracture) for all fractures, for those of the NE set alone, and for those of the NW set alone.

TABLE 2.
FRACTURE DIP DATA FOR TA-21 [a]

Fracture Set	*Number*	*Mean Dip from Vertical (°)*	*Standard Deviation*
All Fractures			
NE	988	9	±27
N	768	17	±24
S	220	-20	±19
NW	674	9	±26
N	559	16	±21
S	115	-25	±21
Background (West)			
NE	182	4	±25
NW	128	6	±21
Fracture Zone			
NE	312	10	±31
NW	212	11	±33
Background			
NE	494	9	±25
NW	334	8	±23

[a] Dips shown in degrees from vertical, southerly dips designated by negative values. Fracture zone corresponds to horizontal distances from 2500 to 4000 ft east of Omega Site.

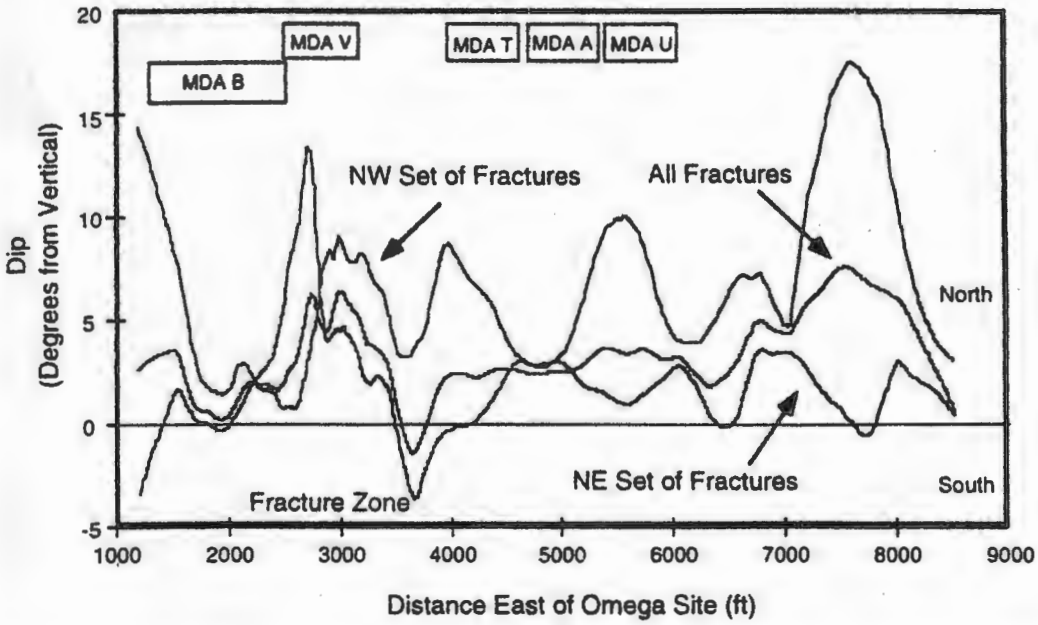

Fig. 6. Plot of fracture dips (relative to vertical at 0°) vs distance east of Omega Site, comparing all fractures to those NW and NE ones. As in Fig. 5, 0.1 smoothed data curves are shown for all fractures, for those of the NE set, and for those of the NW set.

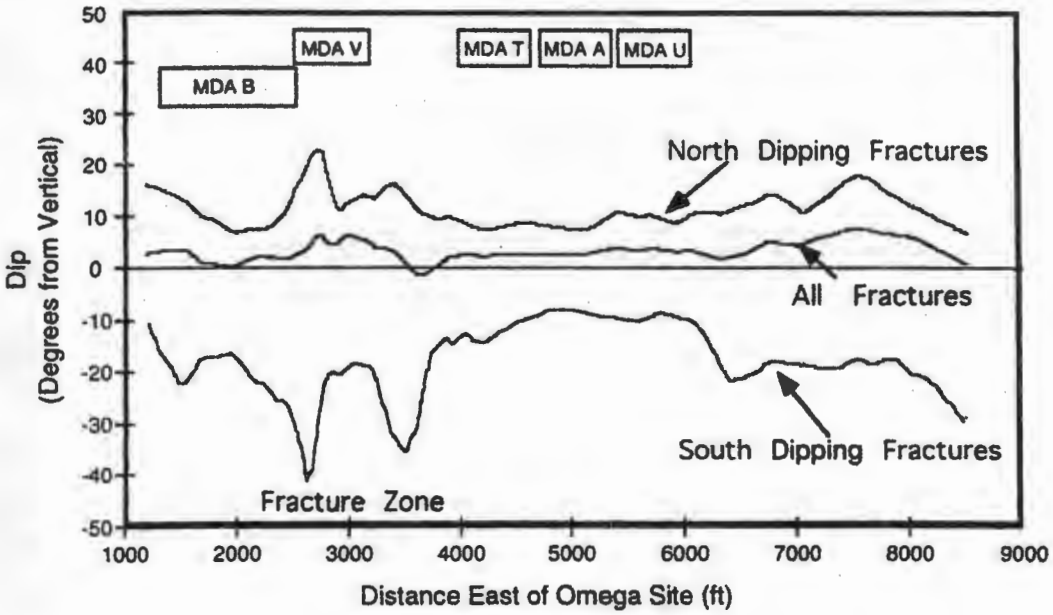

Fig. 7. Plot of fracture dips (relative to vertical at 0°) vs distance east of Omega Site, comparing all fractures to those north- and south-dipping fractures. As in Fig. 5, the 0.1 smoothed data curves are shown for all fractures, for the north-dipping set alone, and for the south-dipping set alone.

dips going east into the fracture zone; east of the fracture zone, they become antithetical and show opposite trends. Figure 7 shows a plot of dips for all fractures, northerly dipping fractures only, and southerly dipping fractures only as a function of horizontal location. For most of the section, as northerly dips become less vertical with distance, so do southerly ones. An increased fluctuation in dip is noted over the fracture zone—again, a possible effect of tectonic movement.

Fracture Apertures

Fracture apertures ranged from 0 cm (closed) to 15 cm (open). Aperture statistics (Table 3) show mean openings of 0.82 and 0.93 cm for the NE and NW sets, respectively; however, the standard deviations of between ±1.08 and ±1.33 cm indicate that most apertures vary between 0 and about 2 cm. Table 3 shows that mean apertures increase from ~0.84 cm west of the fracture zone, to 1.11 cm for the NE set, to slightly more (1.52 cm) for the NW set within the fracture zone. East of the fracture zone, apertures again fall off to mean values around 0.61 cm and standard deviations are about one-half as much as those found to the west of the most highly fractured zone. It is not known to what degree (if any) fracture apertures have been modified by their proximity to the canyon walls. No visible erosive widening was observed; the fractures show more or less pristine, case-hardened surfaces. However, apertures were observed to decrease above and below unit 2. Fracture-filling materials are sparse to absent in unit 2, but they become prominent in unit 3.

Figure 8 is a plot of fracture widths *vs* horizontal location. The data have been smoothed and compared to the linear fracture density curve of Fig. 3. Note the strong correspondence of fracture widths with linear fracture density. From background values of ~ 0.85 cm, fracture widths rise to values >3 cm over the fracture zone. In Fig. 9, cumulative fracture widths for 100-ft intervals centered on each fracture are plotted against horizontal location and compared to the linear fracture density

TABLE 3.
FRACTURE APERTURE DATA [a]

Fracture Set	*Number*	*Mean Aperture (cm)*	*Standard Deviation*
All Fractures			
NE	988	0.8	±1.1
NW	674	0.9	±1.3
Background (West)			
NE	182	0.9	±1.2
NW	128	0.8	±1.1
Fracture Zone			
NE	312	1.1	±1.5
NW	212	1.5	±2.0
Background (East)			
NE	494	0.6	±0.6
NW	334	0.6	±0.6

[a] Fracture zone corresponds to horizontal distances from 2500 to 4000 ft east of Omega Site.

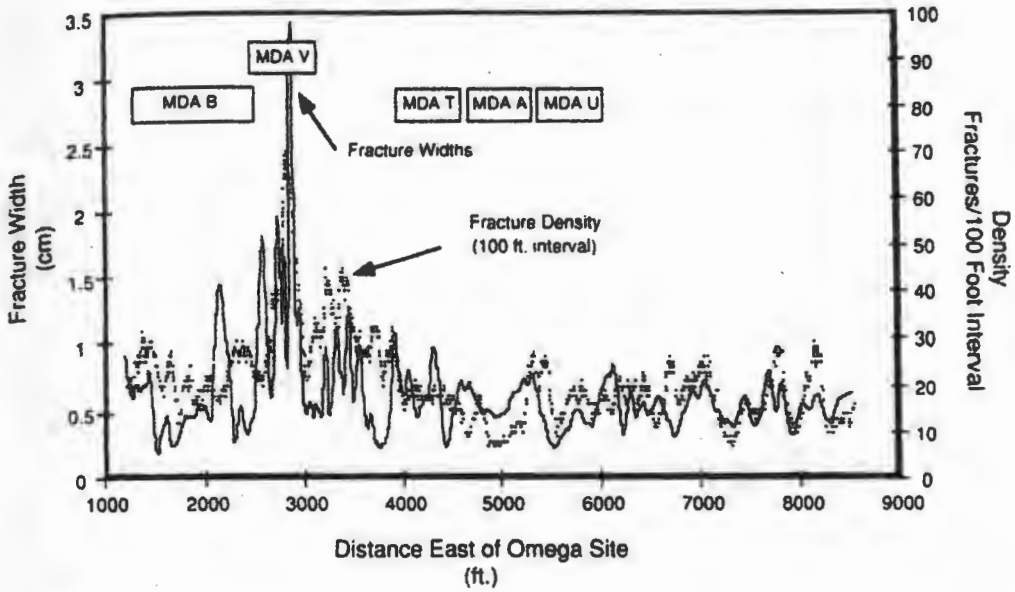

Fig. 8. Plot of fracture widths (apertures) vs distance east of Omega Site compared to linear fracture density from Fig. 3. The fracture data are represented by a 0.2 smoothed curve (81-point moving average).

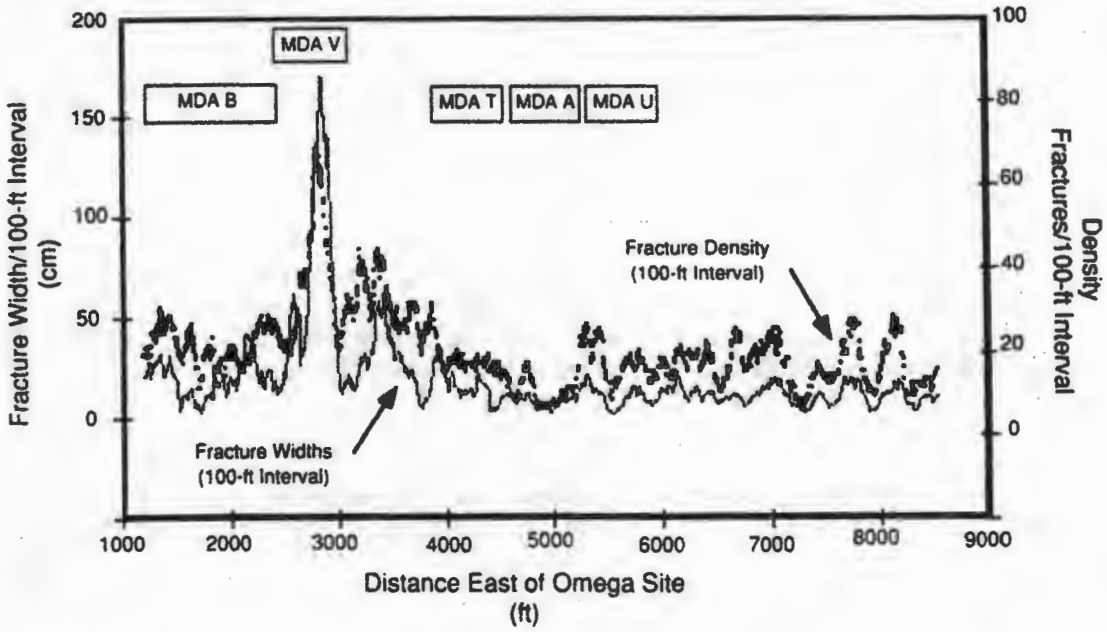

Fig. 9. Cumulative fracture widths over 100-ft interval centered on each fracture plotted against horizontal location.

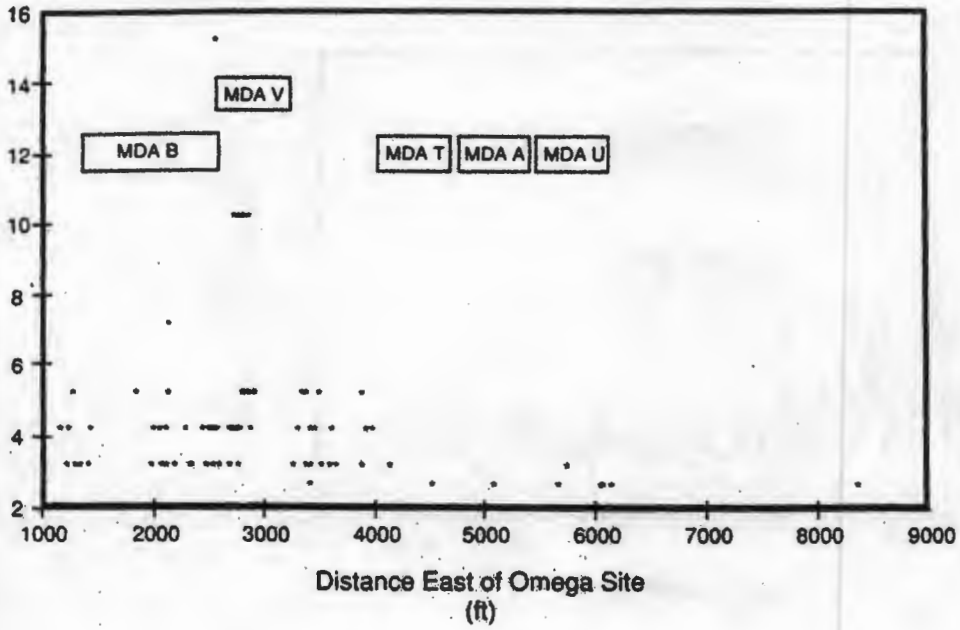

Fig. 10. Fractures with widths >2 cm plotted against horizontal location.

data. From a background of ~0.5 m of fracture opening over 100-ft intervals, the cumulative fracture opening rises to about 1.4 m/100-ft interval over the fracture zone. The importance of the fracture zone with respect to fracture apertures is further emphasized in Fig. 10, where only fractures with openings >2 cm are plotted with location.

CONCLUSIONS

The fracture characteristics described above apply to unit 2 of the Tshirege member, but their similarity to those described by Vaniman and Wohletz (1990) for unit 3 of the Tshirege Member suggests that these results for unit 2 can be extrapolated to the rocks directly underlying TA-21. The results of this present study also support the conclusion that a fracture zone probably related to the Pajarito Fault system runs on a northerly course through MDA-V of TA-21. The fracture zone appears as an area of increased fracture density from 2500 to 4000 ft east of Omega Site. Over this 1500 ft of increased fracture density, there is a cumulative fracture aperture of nearly 6.7 m. It is not known whether tectonic movement produced the increased number of fractures by creating new ones or by opening rock discontinuities originally formed by cooling contraction.

Study of the potential for contaminant migration will be pursued by coring below MDAs. Trigonometric analysis of these fracture data will provide optimum slant-drilling orientations for intersecting the greatest number of fractures in a given length of drill core. From the data in Tables 1 through 3, it is apparent that NE-striking fractures are ~30% more abundant than NW-striking ones. Furthermore, the NE-striking fractures (those that dip north into the NW quadrant) are over three times more abundant than south-dipping ones. Hence, as a first approximation, slant drilling in the direction S48E should

optimize fracture intersections. However, if calculated E-W fractures (Fig. 4b) are realistic, then N-S slant drilling should also be pursued.

This report concludes the field characterization of fracture orientations and apertures for the upper vadose zone at TA-21. The data presented in this report will be used to design drilling programs for characterization of the MDAs. These data will also be used to evaluate the role of fractures in contaminant migration at TA-21. Additional fracture characterization is planned for deep boreholes when the drilling is completed. In addition, there is an ongoing mineralogical study of fracture-lining and fracture-filling minerals at TA-21. The results of the fracture mineralogy studies will be reported separately.

AKNOWLEDGEMENTS

J. Gardner, K. Carter, D. Broxton, and G. Eller provided critical reviews of this paper.

REFERENCES

Gardner, J.N., and House, L., 1987, Seismic hazards investigations at Los Alamos National Laboratory, 1984-1985, Los Alamos National Laboratory report LA-11072-MS, 76 pp. (7 maps, 1:62500 scale).

Vaniman, D., and Wohletz, K., 1990, Results of geological mapping/fracture studies: TA-55 area, Los Alamos National Laboratory Seismic Hazards Memo EES1-SH90-17, 25 pp. (3 plates, map, 1:7800 scale).

LA-12934-MS

Earth Science Investigations for Environmental Restoration—Los Alamos National Laboratory Technical Area 21

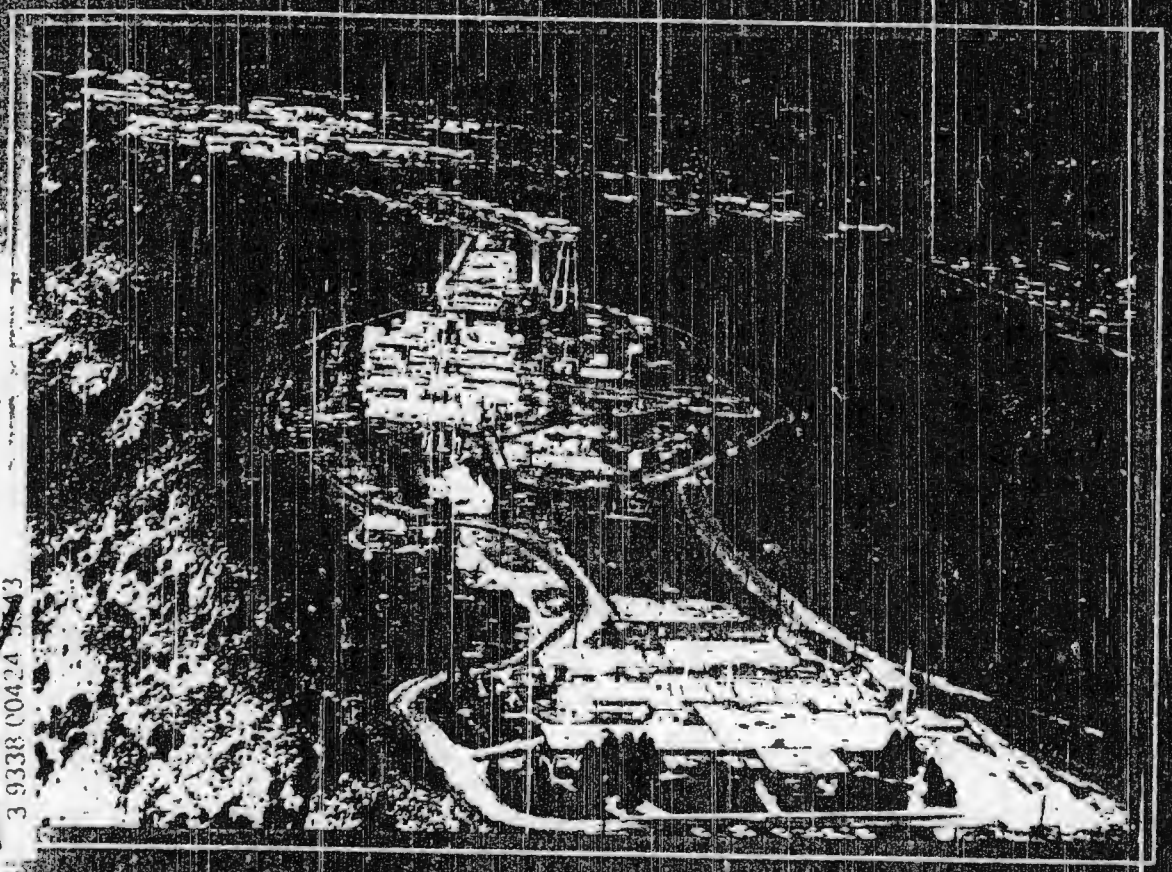

3 9338 00424 [illegible]3

Los Alamos
NATIONAL LABORATORY

Los Alamos National Laboratory is operated by the University of California for the United States Department of Energy under contract W-7405-ENG-36.